Conserved signaling pathways antagonize and synergize with co-opted *doublesex* to control development of novel mimetic butterfly wing patterns

Nicholas W. VanKuren[a,*], Meredith M. Doellman[a], Sofia I. Sheikh[a], Daniela H. Palmer Droguett[a,b], Darli Massardo[a], Marcus R. Kronforst[a]

Affiliations

a: Department of Ecology & Evolution, The University of Chicago, Chicago IL 60637

b: Current address: Department of Biology, The University of Texas at Arlington, Arlington TX 76019

***Corresponding Author**

The University of Chicago

209 Zoology

1101 E 57th Street

Chicago IL 60637

Email: nvankuren@uchicago.edu

Classification

Biological Sciences / Evolution

Keywords

mimicry, development, evolution, sexual dimorphism, gene regulation

ABSTRACT

Novel phenotypes are increasingly recognized to have evolved by co-option of existing gene regulatory networks (GRNs) into new developmental contexts, yet the changes induced by co-option remain obscure. Here we provide insight into the process of co-option by characterizing the consequences of *doublesex* co-option in the evolution of mimetic wing color patterns in *Papilio* swallowtail butterflies. *doublesex* is the master regulator of insect sex differentiation, but has been co-opted to control the switch between discrete female wing color patterns in *Papilio polytes*. We show that a pulse of widespread *dsx* expression early in mimetic wing development activates an alternate color pattern development program that quickly becomes decoupled from *dsx* expression itself. RNAi and antibody stains revealed that Wnt signaling antagonizes *dsx* function in some regions of the wing to refine the mimetic color pattern, but that *dsx* function depends on *engrailed,* the key transcription factor effector of the Hedgehog pathway. Dsx alters spatial patterns of En expression early in pupal development, but the two genes become decoupled by mid-pupal development when En expression pre-figures melanic and red patterns in all *P. polytes*. Co-option of *dsx* into the developing wing therefore results in global changes to development GRNs that function to antagonize and synergize with *dsx* to specify a novel adaptive phenotype. Altogether, our findings provide strong experimental evidence for how co-opted genes cause and elicit changes to GRNs during the evolution and development of novel phenotypes.

SIGNIFICANCE STATEMENT

The diversity of life has been built one mutation at a time, but some mutations have larger effects than others. Recent work has shown that entire developmental programs can be copied and pasted, i.e. co-opted, into new parts of an organism and, with some more evolution, produce novel adaptive traits. This paper describes how *doublesex* was co-opted to produce mimetic color patterns in *Papilio* swallowtail butterflies and shows the role that local developmental pathways play in limiting or synergizing with the co-opted gene to produce a novel trait. Our results have important implications for understanding the evolutionary process by which developmental programs are modified to produce fuel for natural selection.

INTRODUCTION

It is now well appreciated that evolutionary novelties arise from co-option of existing genes and gene regulatory networks (GRNs) into novel contexts, yet the molecular mechanisms underlying this process remain obscure (1–3). Current models describe co-option as a process in which a *cis*-regulatory change confers a novel expression pattern on a regulatory gene that results in activation of the gene and its downstream targets in a novel context, producing a phenotype and developmental program that can be refined by natural selection. Numerous examples exist of *cis*-regulatory mutations leading to co-option and recent studies have begun to deeply characterize the co-opted GRNs themselves (4–6). However, it remains essentially unknown how existing GRNs are modified by the invasion of co-opted GRNs (7).

Classic examples of co-option come from studies of the evolution and development of butterfly wing color patterns, where patterns such as eyespots and bands evolved by the spatial and temporal redeployment of deeply conserved regulatory genes (8–11). Multiple components of ancient signaling pathways such as Hedgehog, Wnt, and Notch have been repeatedly co-opted into developmental programs that function early in wing development to specify novel color patterns (12–16). These genes perform their co-opted functions after they have completed their ancestral functions specifying the major axes of the wing. What has not yet been made clear is how novel expression patterns of these co-opted genes result in correlated changes to existing color pattern networks to produce these new phenotypes.

Here we investigate the developmental genetic basis of *doublesex* co-option in the evolution of female-limited mimicry polymorphism in the swallowtail butterfly *Papilio polytes*. In *P. polytes* and its close relatives, *dsx* has been co-opted from its role as the master regulator of insect sex differentiation to control the switch between female wing color patterns (17, 18). While male *P. polytes* develop a single non-mimetic color pattern, females develop either a male-like pattern or one of several derived mimetic patterns, and the mimicry switch is completely controlled by novel dominant *dsx* alleles (19, 20). Recent work has begun to identify

genes that help execute the mimicry switch, particularly Wnt signaling ligands *wingless* and *Wnt6,* but the GRNs underlying mimetic color pattern development and how *dsx* alleles alter them remain unknown (21, 22).

We experimentally characterize the *dsx* mimicry switch at multiple layers of the color pattern development program. We identify temporal and spatial expression pattern differences between *dsx* alleles, identify differential gene expression and GRN differences associated with the mimicry switch, experimentally test the effects of altered signaling pathways on color pattern development, and perform a detailed study of one key effector of the mimicry switch, *engrailed*. Altogether, our results show that differential *dsx* expression alters the strength and patterning of Wnt and Hedgehog signaling between mimetic and non-mimetic butterflies and that these pathways antagonize and cooperate with *dsx* to produce novel color patterns.

RESULTS

Dynamic Dsx^{H} expression patterns in pupal wings

We first aimed to fully characterize the dynamics of *dsx* expression in the developing wing to understand where and when *dsx* functions during color pattern development. We analyzed hindwings of males and females homozygous for the non-mimetic *dsx*^{h} or mimetic *dsx*^{H} allele, allowing us to disentangle the effects of sex and genotype on *dsx* expression. RNA-seq showed that *dsx* is moderately expressed in male and non-mimetic female hindwings across early- to mid-pupal development, but the mimetic allele undergoes a unique pulse of expression in mimetic females two days after pupation (P2, or 15% pupal development, PD; Fig 1, ref. 18).

We characterized spatial patterns of Dsx expression using antibody stains. Dsx staining was uniform across the wing in all butterflies at 15% PD, with stronger overall staining in mimetic females consistent with RNA-seq data (Fig 1). While non-mimetic Dsx remained weak and uniform across wings in males and females, mimetic Dsx exhibited dynamic expression

patterns in both sexes. By 40% PD in mimetic females, Dsx was restricted to scale and socket cell nuclei in regions that become white, with weaker staining in epidermal cell nuclei in some medial regions that become predominantly red. Stains at intervening days showed a smooth transition between these two general patterns (Fig 1; Fig S1). Mimetic Dsx staining was weak in males from 15% - 40% PD, but was noticeably enriched in scale/socket precursor cell nuclei in regions that become pale yellow (Fig 1; Fig S1). Male expression patterns were surprising because *dsx* RNAi does not alter male color pattern (Dataset S1) and we observed no enrichment in these regions in non-mimetic *dsx* butterflies (Fig 1).

Thus, in addition to the spike of expression early in mimetic female development, the mimetic *dsx* allele has gained novel expression in scale cells and their precursors in regions that become white and pale yellow in adults. Notably, mimetic Dsx expression did not fully pre-figure the mimetic color pattern over the times we investigated, especially red patterns, suggesting that the pulse of widespread *dsx* expression in mimetic female wings activates alternate developmental programs that continue to function in cells after Dsx expression is lost.

An early spike of differential expression alters trajectories of conserved signaling pathway genes

Dsx stains suggested that differences in spatial expression patterns between the two alleles do not explain the color pattern switch, but that the pulse of mimetic *dsx* expression early in pupal development may alter color pattern development programs across the wing. We characterized these changes in gene expression using RNA-seq data from five developmental stages spanning the major phases of color pattern specification (Fig 1B; Table S1; Figs S2-S4).

We identified genes differentially expressed (DE) between mimetic and non-mimetic butterflies using two complementary approaches (Fig 2; Table S2). We found 904 genes DE at one or more developmental stages by analyzing each stage separately, with 98.2% of these stage-specific DE genes coinciding with the pulse of mimetic *dsx* expression. The majority of

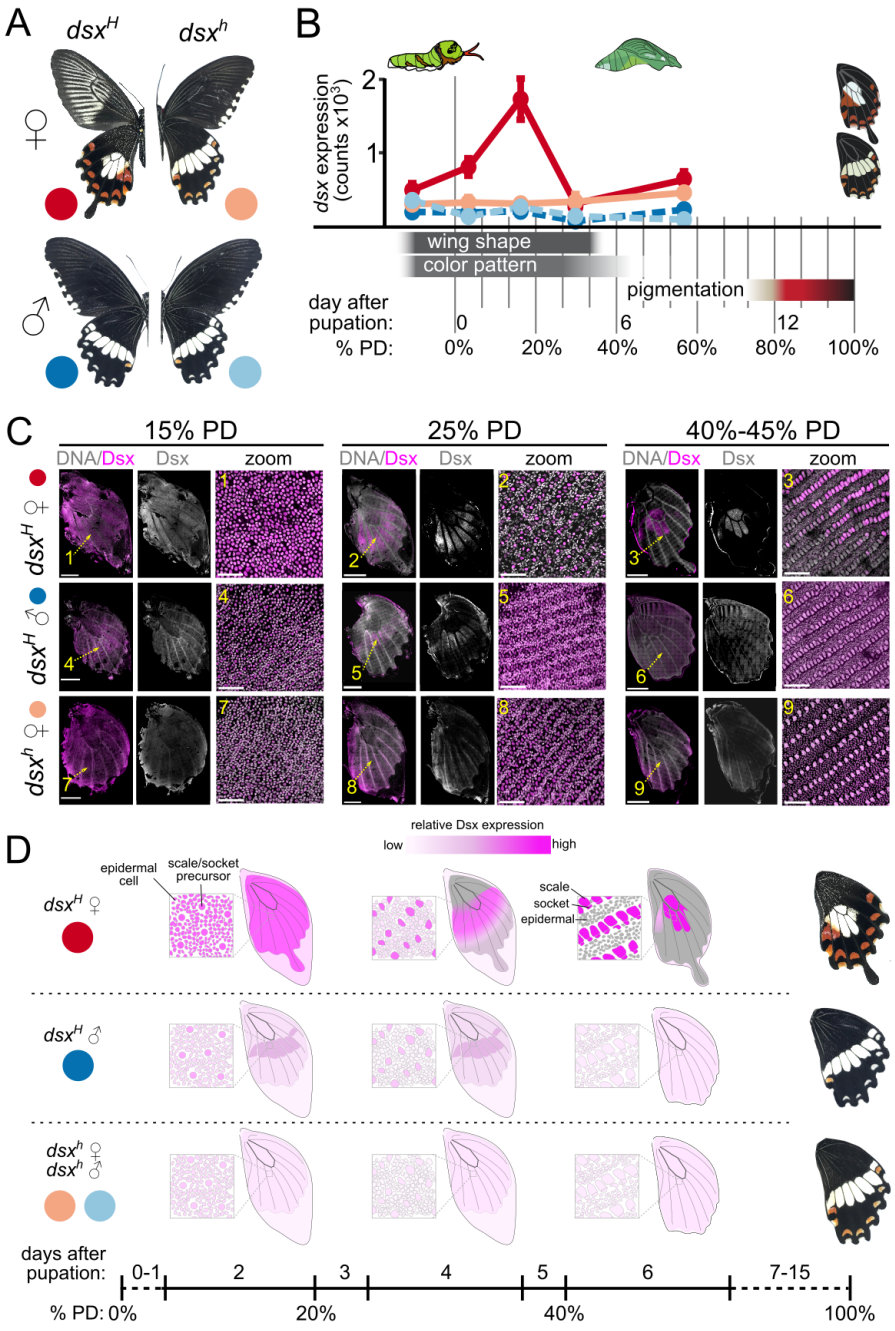

Figure 1. Dynamic *doublesex* expression patterns across *Papilio polytes* hindwing development. A) Adult *Papilio polytes alphenor* color patterns and *dsx* genotypes. B) *dsx* expression in bulk hindwing RNA-seq data in relation to phases of hindwing development. All four major *dsx* isoforms were expressed at each stage in all four groups, but the spike of *dsx* expression was primarily driven by female isoform 2 (Fig S2). C) Anti-Dsx antibody staining at selected stages of hindwing development. Merged images show DNA (gray) and Dsx (magenta). Zoom images are derived from the middle of the wing (between veins M2 and M3 near the discal cell). All images are of the ventral surface. Scale bars: 2 mm for full wings, 50 μm in zooms. D) Schematic of observed Dsx expression patterns. Additional stains can be found in Fig S1.

stage-specific DE genes (65.9%) were down-regulated in mimetic females relative to non-mimetic females (Fig 2A). We also identified 1598 genes with significantly different temporal expression profiles in mimetic females relative to non-mimetic females (878) or all non-mimetic butterflies (720; Fig 2B). Stage-specific and temporal analysis results were largely non-overlapping, with stage-specific tests identifying genes with a single sharp peak or trough in expression and temporal tests identifying genes with subtler expression profile differences (Fig 2C, D). Altogether, these results suggested that the mimicry switch depends on an early spike of *dsx* expression that has both acute and long-term effects on gene expression in developing hindwings.

We placed DE genes into the context of GRNs by reconstructing the hindwing development co-expression network using WGCNA, then identifying sets of co-expressed genes (modules) enriched with DE genes (Fig 2E; Fig S5; Table S3) (23, 24). DE genes were significantly enriched in five of 32 modules (Fig 2; Table S3). These five modules were significantly enriched with Gene Ontology terms associated with gene expression regulation at the levels of both transcription and translation (Fig 2E; Table S3), further supporting the idea that mimetic Dsx causes large-scale alterations to color pattern development networks.

Conserved signaling pathways such as Wnt, Hedgehog (Hh), and Notch have been repeatedly co-opted into wing color patterning networks from their ancestral roles specifying tissue and cellular polarity (8–16). We therefore suspected that the Dsx mimicry switch may depend on altered activities of these pathways. Indeed, DE genes were significantly enriched with canonical Wnt (χ^2 = 8.51, 1 d.f.; p = 0.0035) and Hh (χ^2 = 9.77, 1 d.f.; p = 0.0018) pathway components, including multiple Wnt ligands, core components of the *β-catenin* / *cubitus interruptus* regulator complex, and key transcription factor effectors, altogether suggesting that mimetic Dsx causes a fundamental shift in the strength or pattern of these core signaling pathways across the developing mimetic wing (Table 1; Tables S4-S6).

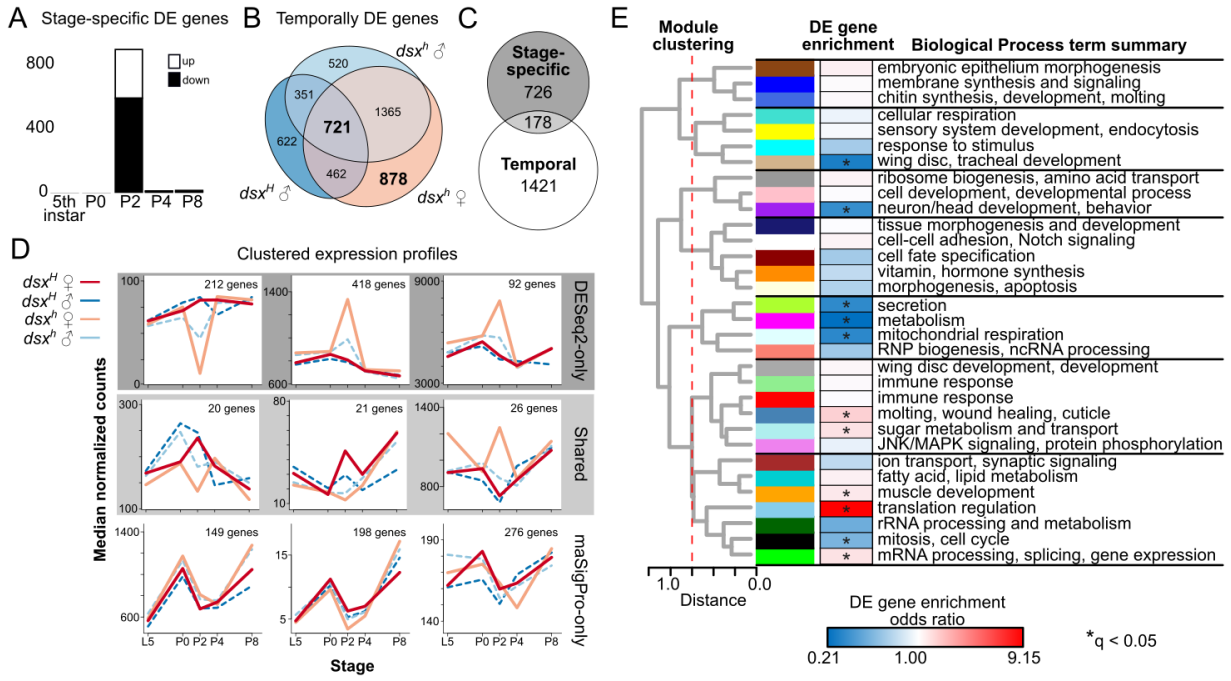

Figure 2. Differential expression associated with the mimicry switch. A) Genes differentially expressed between mimetic and non-mimetic females at each stage, identified using DESeq2 (overall FDR 0.01). Up/down is mimetic relative to non-mimetic females. B) Euler diagram of genes with significantly different expression profiles in mimetic *dsx*^{H} females relative to the indicated groups, identified using maSigPro (overall FDR 0.01). C) Euler diagram of overlap between DESeq2 and maSigPro results. D) Median expression profiles of three largest clusters for each set in C. E) Relationships, DE gene enrichment, and Gene Ontology BP term enrichment of co-expressed gene modules identified using WGCNA (see also Fig S5 and Table S3). Dashed red line indicates cuts to define metamodules (separated by horizontal lines). *Benjamini-Hochberg corrected Fisher Exact Test *p*-value < 0.05.

Table 1. Signaling pathway components DE between mimetic and non-mimetic females[a].

		Hedgehog	Wnt	BMP
Ligands		*hh*	*wg, Wnt6, WntA*	*dpp, gbb*
Regulators[b]	unique	*Gprk2, rdx, rsp, su(fu), wdp*	*Axin, notum, Cow*	*cv-2, irk2, magu, sog*
	shared	*β-TrCP, CBP, CK1α, Cul1, dlp, GSK-3β*		-
Effectors	unique	-	*ebi, pygo*	*schnurri*
	shared		*CtBP, groucho, Mad[c]*	
Targets		*dpp, engrailed, wg, SPOP*	-	-

a: Additional information shown in Tables S4 - S6.
b: Includes regulators of ligand export and signal transduction.
c: Shared between Hh and BMP signal transduction pathways.

Canonical Wnt signaling antagonizes mimetic color pattern development

We next tested whether differential expression of these signaling pathway components caused color pattern differences using RNAi. siRNAs were injected into one hindwing at pupation, then pupae were allowed to finish development and emerge as adults, following ref. (25). This method yields strong, long-lasting, and widespread knockdowns of target genes (Fig S6). Consistent with previous studies, *dsx* RNAi in mimetic females resulted in a complete switch from the mimetic to the non-mimetic color pattern, but no effect on non-mimetic color pattern development in either sex (Fig 3A) (18). Results were similar using siRNAs targeting either exon 3 (all female isoforms) or exon 5 (all isoforms except F2C; Fig S2; Dataset S1).

Previous work established that *wg* and *Wnt6* are required for development of submarginal red patterns and some proximal white patterns in mimetic females (22). We tested the effects of DE genes from across the Wnt and Hh signaling cascades, including: signaling ligands *WntA* and *decapentaplegic*; the shared regulator *GSK-3β* (*shaggy*); transcription factors *ebi, pygopus, engrailed,* and *invected*; and a gene with unknown function, *evm.TU.chr18.639* (Fig 3). RNAi of canonical Wnt components resulted in a striking expansion of red patterns and opal scales, which are typically a rare scale type co-localized with red patches, in mimetic female wings (Fig 3). While *ebi* RNAi resulted in mild increases of red scales and decreases in opal scales in the medial two wing cells, *pygopus* and *GSK-3β* RNAi caused most melanic

scales in the second wing cell to become red; extensive loss of opal scales; and extension of the white patch over central red patterns (Fig 3). *evm.TU.chr18.639* RNAi caused phenotypes similar to *ebi* knockdowns, indicating it may also function in Wnt signal transduction. We observed mild or no effects of RNAi of these genes in non-mimetic butterflies, regardless of their *dsx* genotype (Fig 3; Dataset S1). Thus, these genes appear to normally function to restrict medial red patterns and opal scales that are promoted by the mimetic *dsx* allele. Uniquely, *WntA* RNAi caused massive distal expansion of white/pale patches in all butterflies, suggesting it has a more general role establishing the distal boundaries of those patterns, similar to its function in some Nymphalidae (Fig 3; Dataset S1; ref. 26).

Altogether, RNAi supports a central role of Wnt signaling in antagonizing the effects of the novel mimetic *dsx* allele. This conclusion is supported by 1) few, weak phenotypes from RNAi in non-mimetic butterflies and 2) the fact that RNAi never fully recapitulated the non-mimetic color pattern, except for *dsx* RNAi. If these pathways are active in these same regions in non-mimetic butterflies, then they are not altering default melanic color patterns. There is an enormous amount of cross-talk between the Wnt and Hh pathways (27), from shared regulators such as *GSK-3β* and *CBP* to co-dependent expression of *wg* and *hh* themselves, that could also allow some degree of compensation.

RNAi targeting genes outside of the canonical Wnt pathway affected red and white patterns. RNAi of *decapentaplegic*, a key target of Hh signaling and one of three BMP ligands, yielded a phenotype similar to *GSK-3β* knockdowns, but with stronger effects near the wing margin. *dpp* RNAi also affected margin patterns in non-mimetic butterflies (Fig 3G). In general, we observed few alterations to marginal patterns, but antibody stains in RNAi wings showed this may be due RNAi mostly affecting the middle 50%-75% of the wing (Fig 4C, Figs S6, S7). Finally, RNAi of Hh transcription factor effectors *engrailed* and *invected* had fundamentally different effects on color pattern than the genes discussed so far and we investigated them further below.

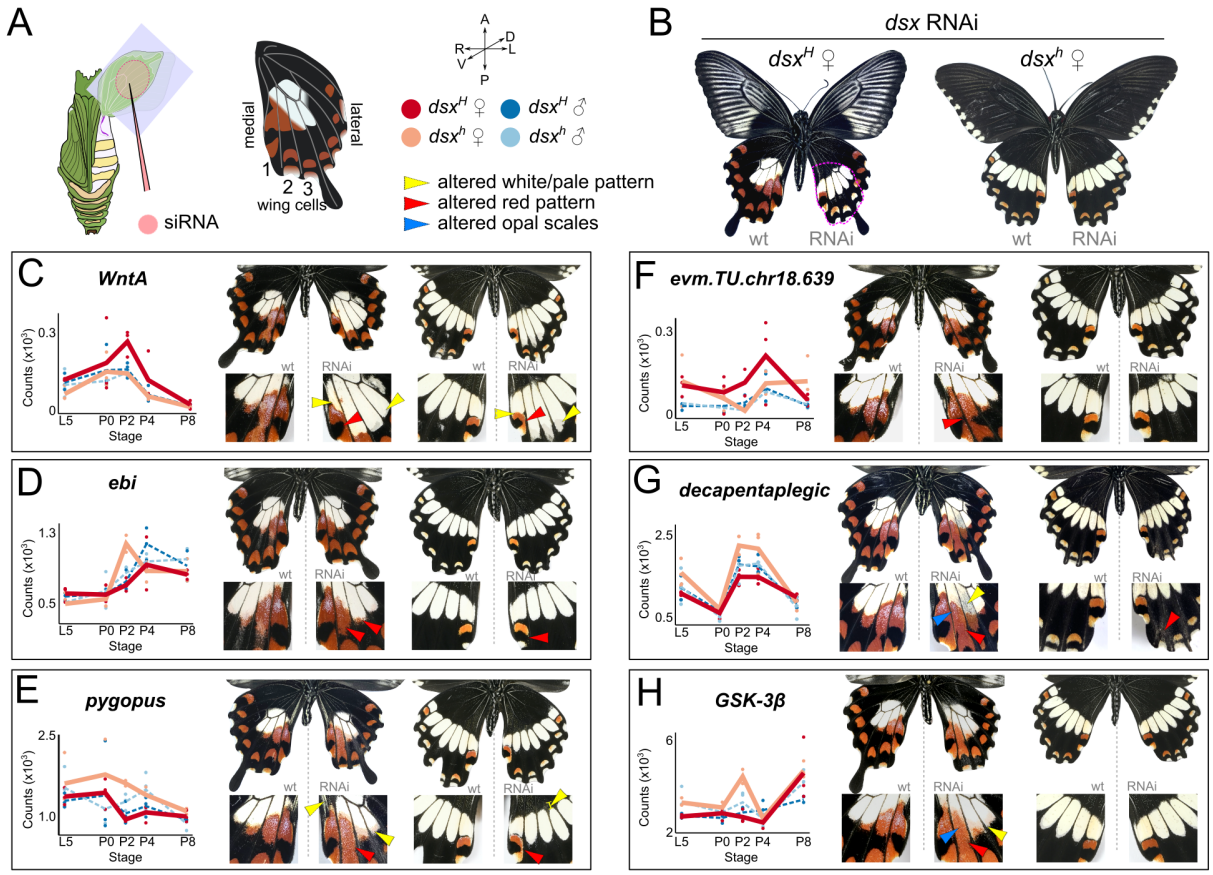

Fig 3. RNAi shows canonical signaling pathways antagonize mimetic Dsx function. A) siRNAs are injected and electroporated into the ventral left hindwing at pupation. Landmarks, orientations, and keys applicable to all panels. B) *dsx* RNAi phenotypes in mimetic and non-mimetic females. The typically affected area is circled in the mimetic female. C-H) Expression patterns from bulk RNA-seq data and phenotypes in mimetic and non-mimetic females for six target genes. All images are of the ventral surface and all comparisons should be made between color patterns on the right wing (wild-type, wt) and left wing (RNAi) of the same individual. Full phenotypes and over 70 additional RNAi individuals are found in the SI.

The Dsx mimicry switch acts through Engrailed

In contrast to RNAi of canonical Wnt components, RNAi of *engrailed* and *invected* caused altered central mimetic patterns that superficially resembled the non-mimetic color pattern (Fig 4A). *engrailed* RNAi had strong effects in all butterflies (Fig 4B). In non-mimetic butterflies, *engrailed* RNAi caused the pale band to shift distally, suggesting that *engrailed* normally specifies the proximal-distal positioning of these windows in the melanic background (Fig 4B). The shape of the pale patches remained mostly unchanged, but the shift could be so severe that marginal and submarginal patterns merged (Dataset S1). In contrast, *en* RNAi in mimetic females caused complete loss of central red patches and restriction of the central white patch to a band reminiscent of the non-mimetic color pattern (Fig 4B). However, this restricted patch comprised primarily opal and gray scales, not white or pale yellow. These gray scales are normally found at the boundaries of white/pale and melanic regions in wild-type wings. The medial red patch now comprised mainly opal scales. Altogether, *en* RNAi strongly suggests this gene gained a novel role in mimetic color pattern development that helps specify the location of novel color pattern elements and alters scale colors within those elements.

Consistent with this idea, we found striking differences in En antibody staining patterns between mimetic and non-mimetic pupal wings. En was expressed in all nuclei of the posterior two-thirds of late larval instar wing discs in all butterflies, consistent with its ancestral role specifying posterior compartments of appendages (Fig S7; refs. 13, 28). Posterior compartment expression was maintained into early pupal development in all butterflies, where En marked epidermal cells (20% PD; Fig 4C). However, En was uniquely expressed in alternating scale/socket precursors across the distal half of the mimetic female wing. Dsx was expressed in all scale/socket precursors in this region, suggesting that Dsx and additional cell non-autonomous signals coordinate this novel En expression domain. *dsx* RNAi caused complete loss of the novel En expression pattern, but did not alter En expression in epidermal cells, showing that the pulse of mimetic *dsx* expression at 15% PD is necessary for En expression in

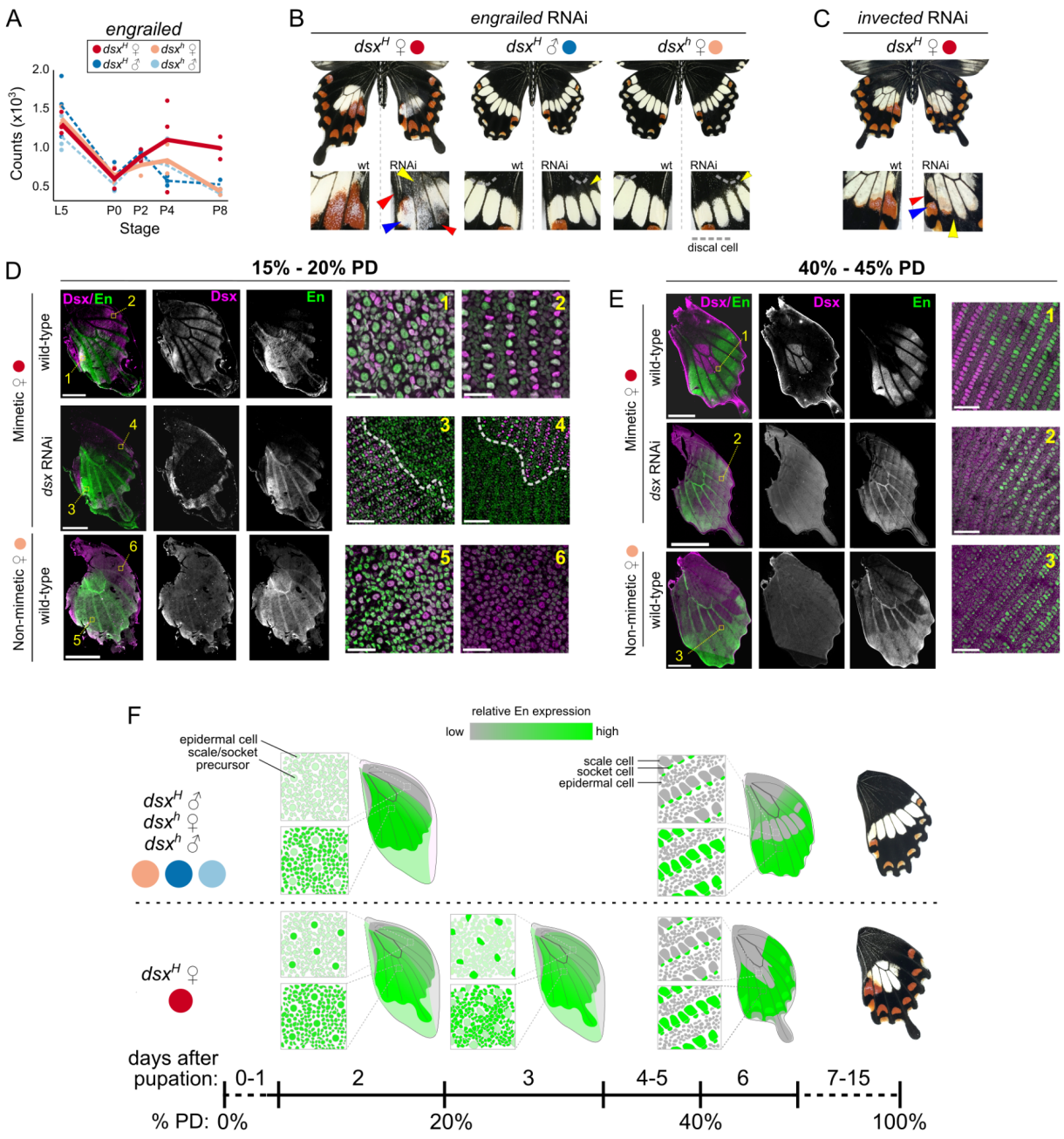

Figure 4. The Doublesex mimicry switch acts through Engrailed. A) Temporal *en* expression patterns. B) *en* RNAi phenotypes. C) *inv* RNAi. D) En and Dsx antibody staining patterns at 15-20% pupal development (PD). Dashed lines mark edges of *dsx* RNAi clones. Pairs of zoom images from the same wing were taken with the same settings and are not adjusted, so brightness levels are comparable. E) En and Dsx antibody staining patterns at 40%-45% PD. Scale bars: 2 mm for full wings; 25 μm for D1, 2, 5, 6; and 50 μm for remaining for zooms. F) Schematic of En expression across early- to mid-pupal hindwing development. See additional stains in Fig S6.

scale/socket precursors (Fig 4). Males carrying the mimetic *dsx* allele also expressed En in some scale/socket precursors in the distal half of the wing, excluding future pale patches, suggesting mimetic *dsx* is not completely impotent in males (Fig S7).

The pulse of *dsx* expression in mimetic females had long-term effects on *en* expression patterns. By 40%-45% PD in non-mimetic butterflies, En expression expanded to scale and socket cells across the wing, with much weaker expression in future pale yellow patches (Fig 4D). En expression was strongest in the distal half of the wing, and slightly higher in future red patches, supporting the *en* RNAi data and the hypothesis that En specifies the proximal-distal positioning of the pale patches in non-mimetic butterflies. En was also expressed in scale cells across the distal half of the wing in mimetic females, but was highly enriched in all future red patches and excluded from Dsx-positive scale cells in the white patch by 45% PD (Fig 4D). *dsx* RNAi in mimetic females resulted in a non-mimetic-like staining pattern where En was only weakly expressed in future pale patches. Thus, by mid-pupal stages En and Dsx expression patterns appear to be decoupled. *en* RNAi did not affect Dsx expression patterns at 20% or 40% PD (Fig S8).

engrailed and *invected* are frequently investigated together because these paralogs are co-regulated in *Drosophila* and loss-of-function of one paralog can be at least partially compensated for by the other. However, the two genes share only 50% coding sequence identity, 19% protein sequence identity, and differentially function in development of numerous fly tissues. We were therefore interested to know if *inv* had also been co-opted into the *dsx* switch. *Papilio polytes engrailed* was DE in mimetic females relative to all non-mimetic butterflies, remaining highly expressed in later developmental stages (Fig 4A). *inv* was not DE, but was slightly elevated in mimetic females at the same stages as *en*. *inv* RNAi also altered the mimetic color pattern, producing a non-mimetic-like pattern in wing cell 1, distal shift of the white patch, and reduced submarginal red patches. Unlike *en* RNAi, we observed no increase in opal or gray scale frequencies. *en* and *inv* therefore both participate in the mimicry switch but to

different degrees. It is unlikely the *en* and *inv* reagents we used cross-reacted because of their high sequence divergence, different RNAi phenotypes, and the observed complete loss of anti-En staining in *en* RNAi wings (Fig S8). *en* and *inv* RNAi and staining patterns altogether suggested these ancient paralogs cooperate with mimetic *dsx* to produce the novel color pattern.

DISCUSSION

Co-opted GRNs are expected to have immediate pleiotropic effects on local developmental programs that must be mitigated for the co-opted allele to be maintained and fixed in the population. However, those effects and the long-term consequences of co-option on the structures and functions of local GRNs remain poorly characterized (7). The ancestral non-mimetic *dsx* allele plays a limited role in color pattern development: it is lowly expressed across the developing wing and *dsx* RNAi has minimal effects on color pattern (Dataset S1)(18, 29). Thus, the novel mimetic allele gained a dynamic expression pattern that altered color pattern development programs. Our results suggest that several molecular mechanisms have evolved to limit the mimetic allele's function since it formed about 1.7 mya (20), including the gain or loss of *cis*-regulatory elements (CREs) that control the pulse and/or spatially restricted expression patterns and canonical Wnt signaling. Our observations that Wnt component RNAi rarely altered non-mimetic color pattern development strongly supports the idea that altered Wnt signaling is a direct result of *dsx* co-option. Interestingly, males also express mimetic *dsx* and exhibit slightly altered *en* expression, suggesting that mimetic *dsx* expression is not fully refined, or cannot be fully refined due to pleiotropy. The *cis*-regulatory differences between the two *dsx* alleles are currently unknown, but will provide crucial insight into the process by which the mimetic *dsx* allele gained its novel expression pattern and how it was refined by subsequent modifications to the color pattern GRN.

Our results suggest a process for mimetic color pattern development that depends on partial suppression of Dsx function by Wnt signaling: a pulse of *dsx* early in development triggers activation of a mimetic color pattern development program whose spatial activity is refined by Wnt and Hh signaling. This resembles a model suggested in a recent preprint by Komata et al. (29), where they suggested that genes near the *dsx* inversion, especially *UXT* and *sir2*, antagonize mimetic *dsx* function. However, *sir2* RNAi caused similar phenotypes to our Wnt pathway RNAi and *sir2* directly interacts with *β-catenin* in vertebrates (30) suggesting this gene may affect color pattern through its effects on Wnt signaling. We could not properly compare our results with previous studies of the mimicry switch due to missing data (22) or different experimental designs (21), but only 32% of genes selected by Iijima et al. were also found DE here. Note that bulk RNA-seq has low power to detect DE in specific color pattern elements. Application of spatial transcriptomics and functional genomics approaches will be critical for assaying *dsx* function and regulation across the developing wing.

Most of the DE genes we found had altered temporal expression profiles, strongly suggesting that the pulse of co-opted *dsx* expression caused a fundamental shift in the regulatory environment early in development that propagated to later stages. This is supported by network and GO analyses (Fig 2). However, our Dsx and En stains suggest that GRN activities at later stages are decoupled from *dsx* itself, showing that even a brief period of co-opted gene activity can significantly alter local regulatory environments. *engrailed* provides unique insight into this process. *engrailed,* and possibly *invected,* pre-figure eyespots and marginal patterns in some nymphalid larval wing discs (9, 16, 31), and were repeatedly co-opted into dipteran color pattern networks (32, 33). Dufour et al. (33) showed that the interactions between genes in the Hh signaling pathway change over wing development, and *engrailed* in particular has been co-opted to produce novel wing color patterns in some Drosophilidae without affecting most other components of the Hh GRN. Interestingly, the novel En expression domain in *P. polytes* does not depend solely on *dsx* because the two genes are not perfectly co-

expressed (Fig 4). Hh and Wnt negatively feed back on each other during segment polarity specification, and this may be another manifestation of that interaction. Importantly, En does not appear to be performing a fundamentally different function in non-mimetic and mimetic color pattern development. Instead, mimetic *dsx* alters the strength and pattern of En expression across the wing to shift the position of non-pigmented windows and the frequency of red scales.

Notably, genetic variation near *engrailed* and *invected* has also been associated with complex female-limited mimicry polymorphism in *Papilio dardanus* (34, 35). Interestingly, the *en* RNAi phenotypes we observed are quite similar to the female-limited color pattern variation observed in *P. dardanus*, where distal expansion and shifts of central white patches distinguish the common morphs *cenea* and *hippocoonides (35)*. The *hippocoonides* allele is completely recessive, perhaps suggesting a lack of *en* expression and reflecting the *P. polytes en* RNAi phenotype.

ACKNOWLEDGEMENTS

We thank Nipam Patel for providing antibodies, The University of Chicago Functional Genomics Facility (RRID:SCR_019196) and its staff for their help with sequencing, the University of Chicago greenhouse staff, and Ayşe Tenger-Trolander, Kelsey Stilson, Erick X. Bayala, and Adam Kuuspalu for technical assistance. This work was funded by NIH R35 GM131828 to MRK.

MATERIALS AND METHODS

Butterfly care and pupa dissection

Papilio polytes alphenor pupae were purchased from Philippines breeders and grown in the University of Chicago greenhouses. Virgins were labeled on the hindwing with permanent marker, then genotyped for *dsx* alleles using a leg and custom TaqMan (Thermo Scientific) assays. Males and females were housed in separate 2 m^3 mesh cages until setting up single-pair crosses between individuals homozygous for mimetic dsx^H or non-mimetic dsx^h alleles. *Citrus* shrubs were provided for oviposition and larval food. Pre-pupae were collected each morning, and photographed to monitor pupation times. Pupae were transferred to an incubator (70% RH, 25°C, 16h:8h light/dark cycle) within 8 hours after pupation (AP) to continue development. A pupa between 12 h and 24 h AP is a day 0 pupa (P0).

Antibodies and staining

We raised a new antibody against *P. polytes* Dsx. We used the protein encoded by the first two exons because they comprise more than 80% of the full protein, are shared between all isoforms, and exhibit 94% identity between *dsx* alleles. Protein synthesis, conjugation, purification, and immunizations were all carried out by GenScript (USA). We confirmed the specificity of this antibody using RNAi and staining in pupal wing discs (Fig 4, Fig S6).

Pupal wings were dissected in room temperature PBS. Cuticle, forewings, and hindwings were dissected out as a single unit. After removing peripodial membranes covering hindwings, wings were fixed for 15 min in 3.7% formaldehyde in PBST (PBS + 0.01% Triton X-100). Wings were washed twice quickly, dissected out from the cuticle and transferred to 4-well plates, then washed 3 x 15 min in PBST. Wings were stored in PBST at 4°C until staining. Wings were blocked in 1% BSA in PBST for 1 hr at RT, then incubated in blocking buffer with primary antibody overnight at 4°C. Wings were washed twice quickly then 5 x 10 min in PBST at RT

before adding secondary staining solution and incubating overnight at 4°C. Wings were washed twice quickly, 5 x 10 min, and 3 x 1 hr in PBST at RT, incubated in 50% glycerol/PBS for 30 min, then covered in Vectashield (Vector Laboratories) until mounting. Antibodies were used at 1:100 (4F11), 1:500 (α-Dsx), or 1:1000 (GαRb AlexaFluor-488, GαRb AlexaFluor-555, DαM AlexaFluor-555, DAPI). Samples were mounted in fresh Vectashield, using double-sided tape to make a coverslip bridge. Images were captured on a Zeiss LSM 710 confocal microscope at the University of Chicago Department of Organismal Biology & Anatomy, then processed using ImageJ. Whole wings were imaged using a 20X objective and a Z-stack / tile scan across the whole wing to capture the entire ventral surface. Images were then stitched and converted to maximum intensity projections in Zen or ImageJ. We took additional images with the 40X objective to characterize cellular localization. Images were assembled and adjusted for brightness and contrast in Inkscape.

RNA-seq library construction and sequencing

Hindwings were dissected out in ice cold PBS, cleaned of peripodial membrane and cuticle, then immediately transferred to RNAlater (Ambion) before storage at -80°C until RNA extraction. One replicate comprised three hindwings from three individuals from a single cross. We extracted total RNA using TRIzol (Ambion), then depleted 18S, 5.8S, 28S, 12S, and 16S rRNAs from each sample using the RNase H method (36). Depleted RNAs were used to construct sequencing libraries using the KAPA RNA HyperPrep Kit (KAPA Biosystems), amplified for 11 cycles, and sequenced 1x50 bp on an Illumina HiSeq 4000 at the University of Chicago Functional Genomics Facility (Table S1).

Differential expression analysis

We assembled and annotated a *Papilio polytes alphenor* genome (see SI Materials and Methods), then quantified transcript expression levels using Salmon v1.4.0 (37) with bias

correction and the full transcript annotation set, then imported and normalized quantification data using tximport 1.18.0 (38) and DESeq2 (39). Differential expression analyses were performed using normalized gene-level quantification data. We identified genes at each developmental stage that respond to the mimetic *dsx* allele specifically in females using DESeq2. We used the following model for these tests, using dsx^h males as the baseline (i.e. sex = 0, genotype = 0):

$$y \sim \beta_0 + \beta_1 \cdot \text{sex} + \beta_2 \cdot \text{genotype} + \beta_3 \cdot \text{sex} \cdot \text{genotype} + \varepsilon$$

We identified genes with significant $\beta_2+\beta_3$ terms, controlling FDR < 0.01 over all five stages. This is equivalent to defining four sex-genotype groups and performing the pairwise comparison between female groups at each stage.

We also identified genes with significantly different temporal expression profiles in mimetic females using *maSigPro* 1.64.0 with a quartic fit (40, 41). Significant genes were selected using a *q*-value cutoff of 0.01 for the p.vector() function, then variable selection performed using *p*-value < 0.05 in T.fit(). Finally, genes with good fits were defined as those with $R^2 > 0.6$. Genes were clustered by expression profile and using maSigPro functions that we modified.

Co-expression network reconstruction and pathway enrichment

We reconstructed the hindwing development gene co-expression network using WGCNA and the gene-level quantification data from above. Adjacency and topological overlap matrices (TOMs) were constructed using signed Pearson coefficients. We performed GO enrichment analyses on each module using topGO v2.44.0 (42) and eggNOG GO assignments (see SI Materials and Methods), utilizing the Fisher Exact Test with adjusted *p*-value < 0.01 to identify

enriched GO categories. We tested for enrichment of canonical Wnt and Hedgehog signaling pathway genes as defined by KEGG pathways 04310 and 04341, respectively. We identified all *alphenor* orthologs of the genes in those pathways using blastp, then performed FETs against all DEGs. The mappings and tests are shown in Tables S4 and S5. We tested whether modules were significantly enriched or deficient in switch genes using FETs.

RNAi

RNAi experiments were performed as described previously by Ando and Fujiwara (25) with small modifications. We designed 24 - 27 nt long Dicer substrate siRNAs (DsiRNAs) using IDT's DsiRNA design tool and the full transcript of the target gene, excluding any designs with off-targets (Table S7). We identified off-targets using primer-BLAST and defined them as any non-target transcripts with fewer than 5 mismatches to the DsiRNA. We injected 1.5 uL of 100 μM DsiRNA into the left hindwing near the discal cell and between veins Cu1 and M3, covered the injected area with PBS, and electroporated into the ventral epithelium using five 0.25 sec, 10V shocks spaced over 5 seconds. Pupae were then placed in an incubator in petri plates with moist paper towels to allow them to finish development or until dissection for stains. Full RNAi results can be found in Dataset S1.

REFERENCES

1. A. Martin, V. Orgogozo, The loci of repeated evolution: a catalog of genetic hotspots of phenotypic variation. *Evolution* **67**, 1235–1250 (2013).

2. D. L. Stern, The genetic causes of convergent evolution. *Nat. Rev. Genet.* **14**, 751 (2013).

3. J. R. True, S. B. Carroll, Gene co-option in physiological and morphological evolution. *Annu. Rev. Cell Dev. Biol.* **18**, 53–80 (2002).

4. S. N. Murugesan, *et al.*, Butterfly eyespots evolved via co-option of the antennal gene-regulatory network https:/doi.org/10.1101/2021.03.01.429915.

5. A. Monteiro, Gene regulatory networks reused to build novel traits: co-option of an eye-related gene regulatory network in eye-like organs and red wing patches on insect wings is suggested by optix expression. *Bioessays* **34**, 181–186 (2012).

6. W. J. Glassford, *et al.*, Co-option of an Ancestral Hox-Regulated Network Underlies a Recently Evolved Morphological Novelty. *Dev. Cell* **34**, 520–531 (2015).

7. E. McQueen, M. Rebeiz, On the specificity of gene regulatory networks: How does network co-option affect subsequent evolution? *Curr. Top. Dev. Biol.* **139**, 375–405 (2020).

8. P. Beldade, P. M. Brakefield, The genetics and evo-devo of butterfly wing patterns. *Nature* **3**, 442–452 (2002).

9. C. R. Brunetti, *et al.*, The generation and diversification of butterfly eyespot color patterns. *Curr. Biol.* **11**, 1578–1585 (2001).

10. P. M. Brakefield, *et al.*, Development, plasticity and evolution of butterfly eyespot patterns. *Nature* **384**, 236–242 (1996).

11. R. D. Reed, *et al.*, optix Drives the Repeated Convergent Evolution of Butterfly Wing Pattern Mimicry. *Science* **333**, 1137–1141 (2011).

12. R. D. Reed, M. S. Serfas, Butterfly wing pattern evolution is associated with changes in a Notch/Distal-less temporal pattern formation process. *Curr. Biol.* **14**, 1159–1166 (2004).

13. R. D. Reed, J. E. Selegue, L. Zhang, C. R. Brunetti, Transcription factors underlying wing margin color patterns and pupal cuticle markings in butterflies. *Evodevo* **11**, 10 (2020).

14. A. Martin, R. D. Reed, Wnt signaling underlies evolution and development of the butterfly wing pattern symmetry systems. *Dev. Biol.* **395**, 367–378 (2014).

15. S. B. Carroll, *et al.*, Pattern formation and eyespot determination in butterfly wings. *Science* **265**, 109–114 (1994).

16. D. N. Keys, *et al.*, Recruitment of a hedgehog regulatory circuit in butterfly eyespot evolution. *Science* **283**, 532–534 (1999).

17. K. Kunte, *et al.*, Doublesex is a mimicry supergene. *Nature* **507**, 229–232 (2014).

18. H. Nishikawa, *et al.*, A genetic mechanism for female-limited Batesian mimicry in Papilio butterfly. *Nat. Genet.* **47**, 405–409 (2015).

19. C. A. Clarke, P. M. Sheppard, The genetics of the mimetic butterfly Papilio polytes. *Philos. Trans. R. Soc. Lond. B Biol. Sci.* **263**, 431–458 (1972).

20. W. Zhang, E. Westerman, E. Nitzany, S. Palmer, M. R. Kronforst, Tracing the origin and evolution of supergene mimicry in butterflies. *Nat. Commun.* **8**, 1269 (2017).

21. R. Deshmukh, D. Lakhe, K. Kunte, Tissue-specific developmental regulation and isoform usage underlie the role of doublesex in sex differentiation and mimicry in Papilio

swallowtails. *R Soc Open Sci* **7**, 200792 (2020).

22. T. Iijima, S. Yoda, H. Fujiwara, The mimetic wing pattern of Papilio polytes butterflies is regulated by a doublesex-orchestrated gene network. *Commun Biol* **2**, 257 (2019).

23. B. Zhang, S. Horvath, A General Framework for Weighted Gene Co-Expression Network Analysis. *Statistical Applications in Genetics and Molecular Biology* **4** (2005).

24. P. Langfelder, S. Horvath, Eigengene networks for studying the relationships between co-expression modules. *BMC Systems Biology* **1** (2007).

25. T. Ando, H. Fujiwara, Electroporation-mediated somatic transgenesis for rapid functional analysis in insects. *Development* **140**, 454 LP–458 (2013).

26. A. Mazo-Vargas, *et al.*, Macroevolutionary shifts of *WntA*function potentiate butterfly wing-pattern diversity. *Proceedings of the National Academy of Sciences* **114**, 10701–10706 (2017).

27. L. Luo, C. K. Siah, Y. Cai, Engrailed acts with Nejire to control expression in the ovarian stem cell niche. *Development* **144**, 3224–3231 (2017).

28. I. Guillén, *et al.*, The function of engrailed and the specification of Drosophila wing pattern. *Development* **121**, 3447–3456 (1995).

29. S. Komata, *et al.*, Functional involvement of multiple genes as members of the supergene unit in the female-limited Batesian mimicry of Papilio polytes. *bioRxiv*, 2022.02.21.480812 (2022).

30. Nguyen, Lee, Lorang-Leins, Trepel, SIRT2 Interacts with β-Catenin to Inhibit Wnt Signaling Output in Response to Radiation-Induced StressSIRT2 Inhibits Wnt Following Radiation-Induced Stress. *Mol. Cancer*.

31. T. D. Banerjee, D. Ramos, A. Monteiro, Expression of Multiple engrailed Family Genes in Eyespots of Bicyclus anynana Butterflies Does Not Implicate the Duplication Events in the Evolution of This Morphological Novelty. *Frontiers in Ecology and Evolution* **8** (2020).

32. N. Gompel, B. Prud'homme, P. J. Wittkopp, V. A. Kassner, S. B. Carroll, Chance caught on the wing: cis-regulatory evolution and the origin of pigment patterns in Drosophila. *Nature* **433**, 481–487 (2005).

33. H. D. Dufour, S. Koshikawa, C. Finet, Temporal flexibility of gene regulatory network underlies a novel wing pattern in flies. *Proc. Natl. Acad. Sci. U. S. A.* **117**, 11589–11596 (2020).

34. M. J. T. N. Timmermans, *et al.*, Comparative genomics of the mimicry switch in Papilio dardanus. *Proceedings of the Royal Society B* **281**, 20140465 (2014).

35. M. J. T. N. Timmermans, A. Srivathsan, S. Collins, R. Meier, A. P. Vogler, Mimicry diversification in Papilio dardanus via a genomic inversion in the regulatory region of engrailed–invected. *Proceedings of the Royal Society B: Biological Sciences* **287**, 20200443 (2020).

36. J. D. Morlan, K. Qu, D. V. Sinicropi, Selective depletion of rRNA enables whole transcriptome profiling of archival fixed tissue. *PLoS One* **7**, e42882 (2012).

37. R. Patro, G. Duggal, M. I. Love, R. A. Irizarry, C. Kingsford, Salmon provides fast and bias-aware quantification of transcript expression. *Nat. Methods* **14**, 417–419 (2017).

38. C. Soneson, M. I. Love, M. D. Robinson, Differential analyses for RNA-seq: transcript-level estimates improve gene-level inferences. *F1000Research* **4**, 1521 (2015).

39. M. I. Love, W. Huber, S. Anders, Moderated estimation of fold change and dispersion for

RNA-seq data with DESeq2. *Genome Biol.* **15**, 550 (2014).

40. A. Conesa, M. J. Nueda, A. Ferrer, M. Talón, maSigPro: a method to identify significantly differential expression profiles in time-course microarray experiments. *Bioinformatics* **22**, 1096–1102 (2006).

41. M. J. Nueda, S. Tarazona, A. Conesa, Next maSigPro: updating maSigPro bioconductor package for RNA-seq time series. *Bioinformatics* **30**, 2598–2602 (2014).

42. A. Alexa, J. Rahnenfuhrer, T. Lengauer, Improved scoring of functional groups from gene expression data by decorrelating GO graph structure. *Bioinformatics* **22**, 1600–1607 (2006).